

Available online at www.elixirpublishers.com (Elixir International Journal)

Nanotechnology

Elixir Nanotechnology 191A (2025) 55151-55157



Phase-Stabilized Y₂O₃/ZrO₂ Nanocomposite with Superior Photocatalytic Degradation Applications

M. Kiruthigadevi^{1*}, R. Mathammal¹, Parikshit Kumar² and Subhadip Senapati²

¹PG & Research Department of Physics, Sri Sarada College for Women (Autonomous), Salem – 636 016, Tamilnadu.

²Prayoga Institute of Education Research, Bangalore – 560085.

ARTICLE INFO

Article history:

Received: 05 July 2025; Received in revised form: 10 August 2025;

Accepted: 29 August 2025;

Keywords

Y₂O₃–ZrO₂ nanocomposite XRD FTIR UV–Visible spectroscopy SEM analysis Photocatalytic Studies Phase Stabilization Environmental Remediation

ABSTRACT

Phase-stabilized Y₂O₃-ZrO₂ nanocomposite were successfully synthesized in two different ratios (60% Y₂O₃-ZrO₂ & 40% Y₂O₃-ZrO₂) and systematically characterized to evaluate their potential for photocatalytic degradation applications. X-ray diffraction (XRD) analysis confirmed the formation of a stabilized cubic/tetragonal zirconia phase with fine crystallite size, indicating the effective incorporation of Y₂O₃ into the ZrO₂ lattice. FTIR spectra revealed the characteristic metal-oxygen vibrational modes associated with Y-O and Zr-O bonding, further supporting the structural stability of the nanomaterials. UV-Visible absorption studies showed a strong absorption edge in the UV region with a reduced band gap, demonstrating enhanced photo-response suitable for photocatalysis. SEM analysis illustrated the formation of uniformly distributed nanosized particles with controlled morphology, which facilitates efficient charge separation during photocatalytic reactions. The photocatalytic studies confirmed that the Y₂O₃-ZrO₂ nanocomposite exhibit superior degradation efficiency toward organic pollutants under UV irradiation, attributed to their improved structural stability, optical activity, and surface morphology. These findings highlight the potential of Y₂O₃-ZrO₂ nanostructures as promising photocatalysts for environmental remediation applications.

© 2025 Elixir All rights reserved.

1. Introduction

The rapid industrialization and urbanization of modern society have resulted in significant environmental challenges, including water contamination by hazardous organic pollutants and the proliferation of pathogenic microorganisms. Developing multifunctional materials that can simultaneously degrade pollutants and exhibit antimicrobial properties has therefore become a key area of research. In this context, metal oxide nanomaterials have emerged as promising candidates due to their unique optical, electronic, and surface properties. Among them, zirconium oxide (ZrO₂), also known as zirconia, has attracted substantial attention owing to its high thermal stability, wide bandgap (5.0-5.5 eV), excellent chemical resistance, and biocompatibility. These properties make ZrO₂ potential material for applications ranging from photocatalysis and biosensing to biomedical coatings and antimicrobial treatments [1-4].

Pure ZrO₂ exists in three main polymorphs monoclinic, tetragonal, and cubic depending on temperature, with monoclinic being the most stable at room temperature. However, the wide bandgap of pure ZrO₂ limits its photocatalytic activity under visible light, as it primarily responds to ultraviolet (UV) irradiation. To enhance its optical absorption, surface reactivity, and defect density, doping with rare-earth elements has been extensively investigated. Among various dopants, yttrium oxide (Y₂O₃) is one of the most effective stabilizers for ZrO₂. Y₂O₃ introduces oxygen vacancies, stabilizes the tetragonal or cubic phases at room

temperature, and improves charge separation by suppressing electron–hole recombination. These modifications collectively enhance the photocatalytic efficiency of ZrO₂ under UV and, in some cases, visible-light irradiation [5, 6].

In addition to improved photocatalytic performance, Y₂O₃-ZrO₂ nanocomposite have demonstrated the synergistic effects of Y₂O₃-ZrO₂ composite not only increase surface area and active sites but also enhance redox potential, thereby amplifying the excellent photocatalytic efficacy of ZrO₂-based nanocomposite. The synthesis of Y2O3-ZrO2 nanocomposite can be achieved through various methods such as sol-gel, hydrothermal, co-precipitation, and solid-state techniques, allowing precise control over particle size, morphology, and phase composition. Tailoring these parameters is crucial because photocatalytic are strongly dependent on crystallite size, surface defects, and electronic structure. Moreover, the biocompatibility and chemical inertness of zirconia-based materials make them suitable for environmentally friendly applications, including water purification, self-cleaning surfaces, and antimicrobial coatings for medical devices.

Given these advantages, Y_2O_3 -Zr O_2 nanocomposite represent a promising class of multifunctional materials. Systematic studies focusing on the correlation between synthesis route, structural properties, and functional performance are essential to optimize their efficiency for real-world applications. This work therefore investigates the structural, optical, photocatalytic characteristics of pure ZrO_2 ,

pure Y_2O_3 , Y_2O_3 - ZrO_2 nanocomposite, with the aim of elucidating the role of yttrium in enhancing their multifunctional performance [7-8].

2. Experimental procedure

2.1. Synthesis of Pure ZrO₂, Pure Y₂O₃ and Y₂O₃-ZrO₂ Nanocomposite

Pure ZrO₂ and Y₂O₃-ZrO₂ nanocomposite were synthesized via a hydrothermal method. In a typical procedure, commercially available ZrO2 was dissolved in 50 mL of solution of oxalic acid dihydrate under continuous magnetic stirring. The appropriate amount of Y₂O₃ corresponding to the desired Y3+ molar ratio (e.g., 1-7 mol% relative to total cations) was slowly added to the zirconium solution with stirring to ensure homogeneous mixing. 10ml of isopropyl alcohol is added to the mixed solution, resulting in the formation Y₂O₃-ZrO₂composite. The suspension was stirred for an additional 30 min to achieve uniformity of the synthesised sample and then transferred into a 100 mL Teflon-lined stainless-steel autoclave, filling about 70-80% of its capacity. The autoclave was sealed and maintained at 150°C for 12h to facilitate hydrothermal crystallization. After naturally cooling to room temperature, the product was collected and washed repeatedly with deionized water and ethanol to remove impurities, and dried at 100°C. To improve crystallinity and phase purity, the dried powder was calcined at 700°C for 6 h. The obtained samples were gently ground to fine powders and stored in a desiccator for subsequent structural, optical, photocatalytic characterizations.

3. Results and Discussion

3.1. X-ray Diffraction (XRD) Analysis

X-ray diffraction (XRD) analysis was carried out to investigate the crystalline structure, phase composition, and average crystallite size of the synthesized pure ZrO2 and Y₂O₃-ZrO₂ nanocomposite is shown in figure 1. For ZrO₂ the more intense peak appeared at $2 = 30.52^{\circ}$ with characteristic crystal plane at (101). The highest peaks were at 30.52°, 35.27°, 50.66°, 60.20°, 63.07°, 74.84°, which corresponded to the tetragonal structure of ZrO₂ reflections (101), (110), (020), (121), (202), and (220) (JCPDS card No. 80 - 0965). The novel formation of secondary phase and the phase transition of ZrO₂ were occurring at 700°C, which results in the monoclinic to tetragonal phase transformation along with an increase in crystallinity. The diffraction patterns of pure ZrO2 exhibited well-defined and sharp peaks, indicating the formation of a highly crystalline material. The presence of these characteristic peaks confirmed that the synthesized zirconium oxide nanoparticles predominantly crystallized in the monoclinic phase at room temperature.

Upon yttrium oxide (Y_2O_3) , distinct changes were observed in the XRD patterns. The diffraction peaks became slightly broader and exhibited a small shift towards lower 2θ angles, which can be attributed to the incorporation of Y^{3+} ions into the ZrO_2 lattice. This substitution causes lattice distortion due to the difference in ionic radii between Zr^{4+} (0.84 Å) and Y^{3+} (0.90 Å), resulting in a slight expansion of the crystal lattice. Moreover, the relative intensity of the monoclinic peaks decreased with increasing Y_2O_3 content, while new peaks corresponding to the tetragonal/cubic phases of ZrO_2 emerged (JCPDS card No. 50-1089 for tetragonal phase). This phase transformation is consistent with the well-known role of Y_2O_3 as a stabilizer that suppresses the monoclinic-totetragonal phase transition at lower temperatures, thereby

stabilizing the high-temperature tetragonal/cubic phases even at room temperature. The average crystallite size of the synthesized nanomaterials was calculated using the Debye–Scherrer equation:

Scherrer equation:

$$D = \frac{k\lambda}{\beta \cos \theta} nm$$
(1)

 θ is the Bragg diffraction angle.

The calculated average crystallite size for pure ZrO_2 and pure Y_2O_3 was found to be in the range of 14 nm, whereas Y_2O_3 - ZrO_2 composite led to a slight reduction in crystallite sizearound 13-13.36 nm for both the ratios, which can be ascribed to lattice strain induced by Y_2O_3 incorporation and inhibition of grain growth [9,10]. The observed reduction in crystallite size is advantageous for photocatalytic applications, as smaller crystallites provide a higher specific surface area, more active sites, and improved generation of reactive oxygen species (ROS).

The absence of any additional impurity peaks related to unreacted precursors or secondary phases of yttrium oxide confirmed the successful incorporation of Y^{3+} into the ZrO_2 lattice, resulting in a single-phase nanocomposite material. The combined effect of lattice distortion, phase stabilization, and crystallite size reduction is expected to enhance photocatalytic performance by facilitating efficient charge separation and migration, as well as promoting higher surface reactivity. Overall, XRD analysis confirmed that Y_2O_3 - ZrO_2 of both the ratios tunes its crystallite size and lattice parameters, which key structural factors, are contributing to its superior photocatalytic performance.

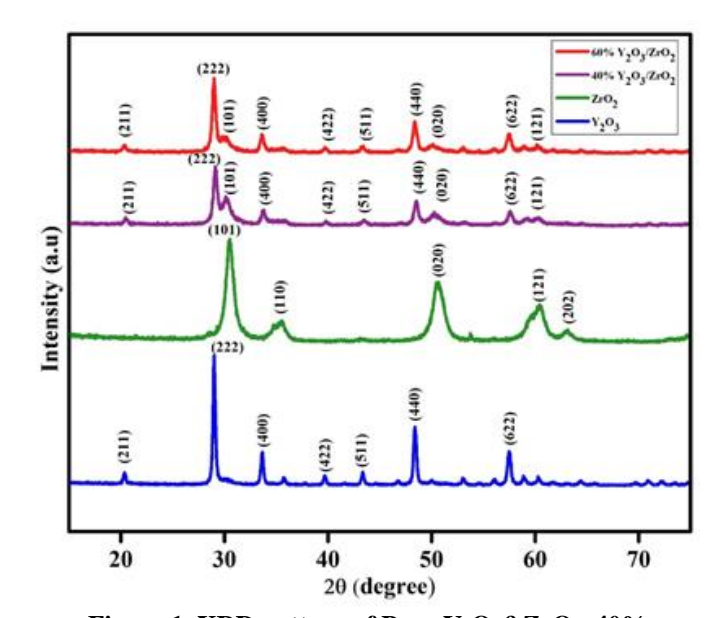


Figure 1. XRD pattern of Pure Y₂O₃&ZrO₂, 40% Y₂O₃/ZrO₂, 60% Y₂O₃/ZrO₂, nanocomposite. 3.2. UV-Visible Diffuse Reflectance Spectroscopy (UV-Vis DRS) Analysis

The optical absorption properties of pure ZrO_2 and Y_2O_3 - ZrO_2 nanocomposite were investigated using UV–Visible diffuse reflectance spectroscopy (UV–Vis DRS) in the wavelength range of 200–800 nmis shown in figure 2. The reflectance spectra of both pure and composites is shown in figure which is recorded in the range of 200 nm to 1400 nm at room temperature.

$$F(R) = \frac{1 - R^2}{2R} \tag{2}$$

Where, F(R) - Kubelka–Munk function, R - Reflectance. The optical energy gap are determined by applying the tauc's relation equation derived from the Kubelka – Munk function. F(R) $h\nu = A (h\nu - E_g)^2$ (3)

For Y_2O_3 , a noticeable red-shift in the absorption edge was observed in the DRS spectra, can be attributed to the incorporation of Y^{3+} ions into the ZrO_2 lattice, which introduces oxygen vacancies and localized defect states near the conduction band. These defect levels act as intermediate energy states, enabling sub-bandgap optical transitions and extending the light absorption into the near-UV and partially visible region. Enhanced visible-light absorption is advantageous for photocatalysis as it allows better utilization of the solar spectrum, thereby improving the generation of electron-hole pairs under natural sunlight or low-energy irradiation [11,12].

For pure ZrO₂, the calculated direct bandgap was found to be 3.88 eV. The diffuse reflectance spectra of pure ZrO₂ exhibited a sharp absorption edge in the deep UV region, characteristic of its wide bandgap semiconductor nature. This strong UV absorption arises from charge transfer transitions between the O 2p valence band and the Zr 4d conduction band. However, due to its large intrinsic bandgap shows negligible absorption in the visible region, which limits its efficiency under solar irradiation for photocatalytic applications. The broader optical band gap of the Y₂O₃ (~5.45 eV) than ZrO₂ (~3.88 eV) can be attributed to the intrinsic electronic structure of yttrium oxide. The conduction band of Y₂O₃ is dominated by Y 4d, which has a higher energy and weaker interaction with O 2p, leading to a larger O 2p-Y 4d splitting. Furthermore, the more ionic Y-O bond and crystal structure decrease orbital hybridization and result in a larger band gap as compared to the more covalent Zr-O bonds in zirconia (ZrO₂) (13,14). Interestingly, Y₂O₃-ZrO₂ nanocomposites exhibited slightly lower bandgap values in the range of 5.25 - 5.32 eV for 40% Y₂O₃-ZrO₂ and 60% Y₂O₃-ZrO₂, confirming the slightly lower bandgap thanpure Y₂O₃. This slight narrowing bandgapis beneficial for photocatalytic degradation of organic pollutants because it enhances photon absorption efficiency and facilitates photoinduced charge carrier generation under lower-energy illumination. This improvement was attributed to the formation of Y₂O₃-ZrO₂heterojunction which facilitates interfacial charge separation and suppresses the electron-hole recombination. The strong coupling between two oxide phases causes directional charge transfer due to favorable band alignment and consequently the lifetime of the photogenerated carriers is extended and reactive oxygen species such as OHand O₂- radicals are generated efficiently. Furthermore, partial substitution of Y3+ ions and the resulting lattice distortion are expected to lead to oxygen vacancies and surface hydroxyl groups which can further increase the dye adsorption and activation sites. This is crucial for improving the yield of reactive oxygen species (ROS) such as •OH and O2•, which are responsible for the oxidative degradation of pollutants.

Therefore, the Y_2O_3 -Zr O_2 composite can lead to stronger oxidative stress, enhanced light absorption and efficient ROS generation. This synergistic effect of improved optical properties and defect engineering underscores the superior photocatalytic Y_2O_3 -Zr O_2 nanocomposite compared to their pure counterparts. UV–Vis DRS analysis confirmed that

 Y_2O_3 -Zr O_2 nanocomposite successfully tailors the optical response by reducing its bandgap, increasing visible-light absorption, and introducing defect states favorable for enhanced photocatalytic activity.

3.3. Fourier Transform Infrared (FTIR) Spectroscopy Analysis

Fourier Transform Infrared (FTIR) spectroscopy was performed to identify the functional groups, bonding vibrations, and chemical interactions present in the synthesized pure ZrO2 and Y2O3-doped ZrO2 nanocompositesis shown in figure 3. The FTIR spectra were recorded in the range of 400-4000 cm⁻¹. For pure ZrO₂, the FTIR spectrum displayed a series of characteristic absorption bands confirming the formation of zirconium oxide. The most prominent and broad absorption peak was observed in the low wavenumber region between 400-700 cm⁻¹, which can be attributed to the stretching vibrations of Zr-O bonds monoclinic/tetragonal ZrO2 lattice. This band is considered the fingerprint region for zirconium oxide and confirms successful synthesis of ZrO2 nanoparticles. A medium-intensity band around 3400-3500 cm⁻¹ was observed, corresponding to the stretching vibrations of surface -OH groups and adsorbed moisture, whereas the band around 1630-1650 cm⁻¹ is ascribed to the bending mode of molecular water (H-O-H bending vibration). The presence of hydroxyl groups on the surface is beneficial, as they act as active sites for the adsorption of pollutant molecules and play a crucial role in the generation of hydroxyl radicals (•OH) during photocatalysis [15, 16].

Upon Y_2O_3 -Zr O_2 composite, noticeable changes appeared in the FTIR spectra. The intensity of the Zr–O stretching vibration peaks slightly shifted and broadened, indicating successful incorporation of Y^{3+} ions into the Zr O_2 lattice and the creation of oxygen vacancies. These structural modifications lead to slight distortion of the crystal lattice, which is reflected as peak broadening in the FTIR spectrum. Additionally, a weak absorption band around $500-600~\text{cm}^{-1}$ can be attributed to Y–O vibrations, further confirming the presence of yttrium oxide in the composite. The increase in intensity of –OH stretching vibrations after doping suggests an increase in surface hydroxyl groups, which enhances surface hydrophilicity and promotes higher photocatalytic activity by facilitating the generation of reactive hydroxyl species under UV/visible light irradiation.

The presence of oxygen vacancies, as indirectly indicated by changes in Zr–O bond vibrations, plays a key role in charge carrier separation by acting as electron traps. These vacancies not only improve photocatalytic efficiency. The strong Zr–O and Y–O bonding vibrations in thenanocomposite confirm the stability of the material, which is important for repeated cycles of photocatalytic reactions. Overall, FTIR analysis confirmed the successful synthesis of pure and $Y_2O_3\text{-}ZrO_2$ nanocomposite and revealed structural modifications. The enhancement in surface hydroxyl groups and the creation of lattice defects are expected to synergistically improve both photocatalytic degradation of pollutants, making $Y_2O_3\text{-}ZrO_2$ composite a promising multifunctional nanocomposite.

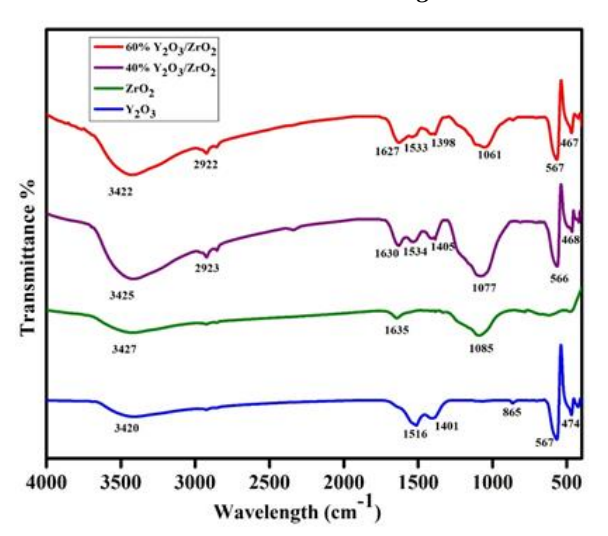


Figure 3. FTIR spectrum of Pure Y₂O₃&ZrO₂, 40% Y₂O₃/ZrO₂, 60% Y₂O₃/ZrO₂

3.4. Scanning Electron Microscopy (SEM) Analysis

The surface morphology of pure ZrO₂ and Y₂O₃-doped ZrO₂ nanocomposites was investigated using Scanning Electron Microscopy (SEM)is shown in figure 4. The SEM images of pure ZrO2 revealed irregularly shaped particles with agglomeration, characteristic of metal nanoparticles synthesized via hydrothermal routes. The surface appeared rough with uneven grain boundaries, indicating a high surface area favorable for catalytic and adsorption processes. The Y₂O₃-ZrO₂ compositeshowed significant morphological changes. The nanocomposites exhibited a more and compact morphology with agglomeration, suggesting that Y3+ ions act as a stabilizing agent, promoting controlled grain growth. The doping process led to smaller particle sizes and a more homogeneous distribution, which is beneficial for enhancing surface reactivity and mechanical stability [17, 18].

A closer examination of the SEM images revealed that Y_2O_3 - ZrO_2 composites significantly influenced microstructural features of both the pure. The nanocomposites displayed a finer grain structure with reduced surface defects compared to both the pure, indicating enhanced structural uniformity. This improvement is attributed to the incorporation of Y3+ ions, which inhibit excessive grain growth and promote densification. Furthermore, the Y₂O₃-ZrO₂ samples exhibited improved particle connectivity and a smoother surface morphology, which can enhance mechanical strength and catalytic performance. These morphological improvements suggest that Y₂O₃-ZrO₂ composite effectively tailors the microstructure for advanced functional applications.

3.5 Photocatalytic Degradation Analyses

The photocatalytic activities of pure ZrO_2 and Y_2O_3 - ZrO_2 nanocomposite were systematically investigated by monitoring the degradation of a model organic pollutant under UV/visible light irradiation. Typically, dyes such as EY (eosin yellow) were selected as representative contaminants due to their stability, well-defined absorption peaks, and ease of detection using UV–Visible spectroscopyis shown in figure 5. Prior to irradiation, the photocatalyst–dye suspension was magnetically stirred in the dark for 30–60 minutes to ensure adsorption–desorption equilibrium between dye molecules and

the photocatalyst surface. Upon illumination, a gradual decrease in the characteristic absorption peak intensity of the dye was observed, indicating effective photocatalytic degradation. Pure ZrO₂ showed moderate photocatalytic activity, consistent with its wide bandgap, which restricts its photoresponse primarily to the UV region. However, Y₂O₃-ZrO₂ nanocomposites exhibited significantly enhanced photocatalytic performance, as evidenced by a faster decline in dye concentration over time. The enhanced activity can be attributed to several key factors introduced by yttrium doping: Bandgap Narrowing and Extended Light Absorption: UV-Vis DRS analysis revealed a slight red-shift in the absorption edge of doped samples, indicating a reduction in bandgap energy. This enables more efficient utilization of incident photons, improving electron-hole generation under UV and near-visible light irradiation.

Oxygen Vacancy Formation and Charge Separation: Y³⁺ substitution for Zr⁴⁺ creates charge imbalance in the lattice, leading to the formation of oxygen vacancies. These vacancies act as shallow electron traps, suppressing electron—hole recombination and thereby prolonging the lifetime of photoexcited charge carriers.

Increased Surface Hydroxyl Groups and Active Sites: FTIR analyses confirmed enhanced surface hydroxylation in doped nanocomposites, which provides additional reaction sites for hydroxyl radical (•OH) formation one of the primary oxidizing species responsible for organic pollutant degradation. While compared to pure ZrO₂, confirming faster degradation kinetics and superior catalytic efficiencyis shown in figure 6. A possible mechanism for the photocatalytic process can be described as follows: upon light irradiation, electrons (e⁻) are excited from the valence band (VB) to the conduction band (CB), leaving behind holes (h⁺) in the VB. The photogenerated electrons react with dissolved oxygen molecules to produce superoxide radicals (O2..), while holes react with surface hydroxyl groups or adsorbed water molecules to produce hydroxyl radicals (•OH). These reactive oxygen species are highly oxidative and attack the chromophoric structure of the dye, leading to stepwise degradation into smaller intermediates and eventual mineralization into CO₂, H₂O, and other nontoxic end products.

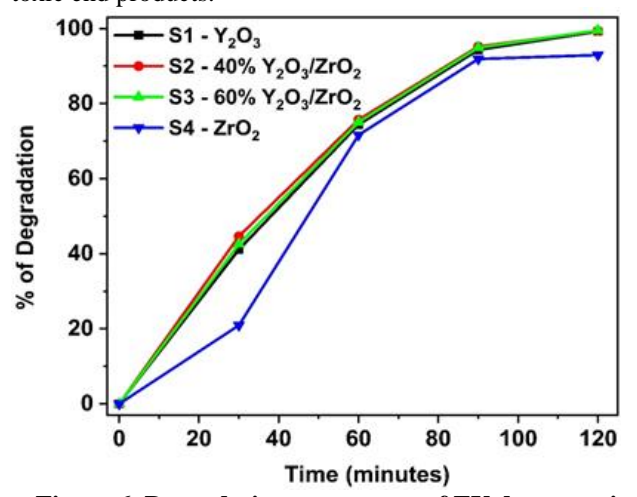


Figure 6. Degradation percentage of EY dye over time with different concentrations of catalysts Pure Y₂O₃ (S1), 40% Y₂O₃/ZrO₂ (S2), 60% Y₂O₃/ZrO₂ (S3), ZrO₂ (S4)

Overall, photocatalytic degradation analysis clearly demonstrated that Y₂O₃-ZrO₂ composite significantly boosts the photocatalytic performance than pure, making it a promising multifunctional material for environmental remediation applications and significantly modifies the photocatalytic mechanism and overcomes these limitations. Y³⁺ ions substitute for Zr⁴⁺ in the ZrO₂ lattice, leading to charge imbalance and the formation of oxygen vacancies for charge compensation. These oxygen vacancies act as shallow electron traps that reduce the rate of electron-hole recombinationis shown in figure 7, thereby prolonging the lifetime of charge carriers and increasing their participation in surface reactions. Additionally, Y₂O₃-ZrO₂ composite slightly narrows the bandgap and introduces localized energy states near the conduction band, allowing better light harvesting under UV and near-visible irradiation [19-21].

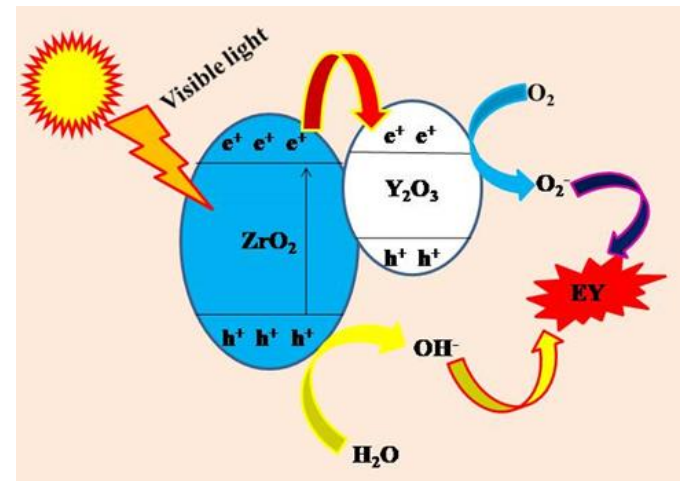


Figure 7. Photocatalytic Mechanisms of degradation of EY (eosin yellow) dye utilizing a catalyst in the presence of light

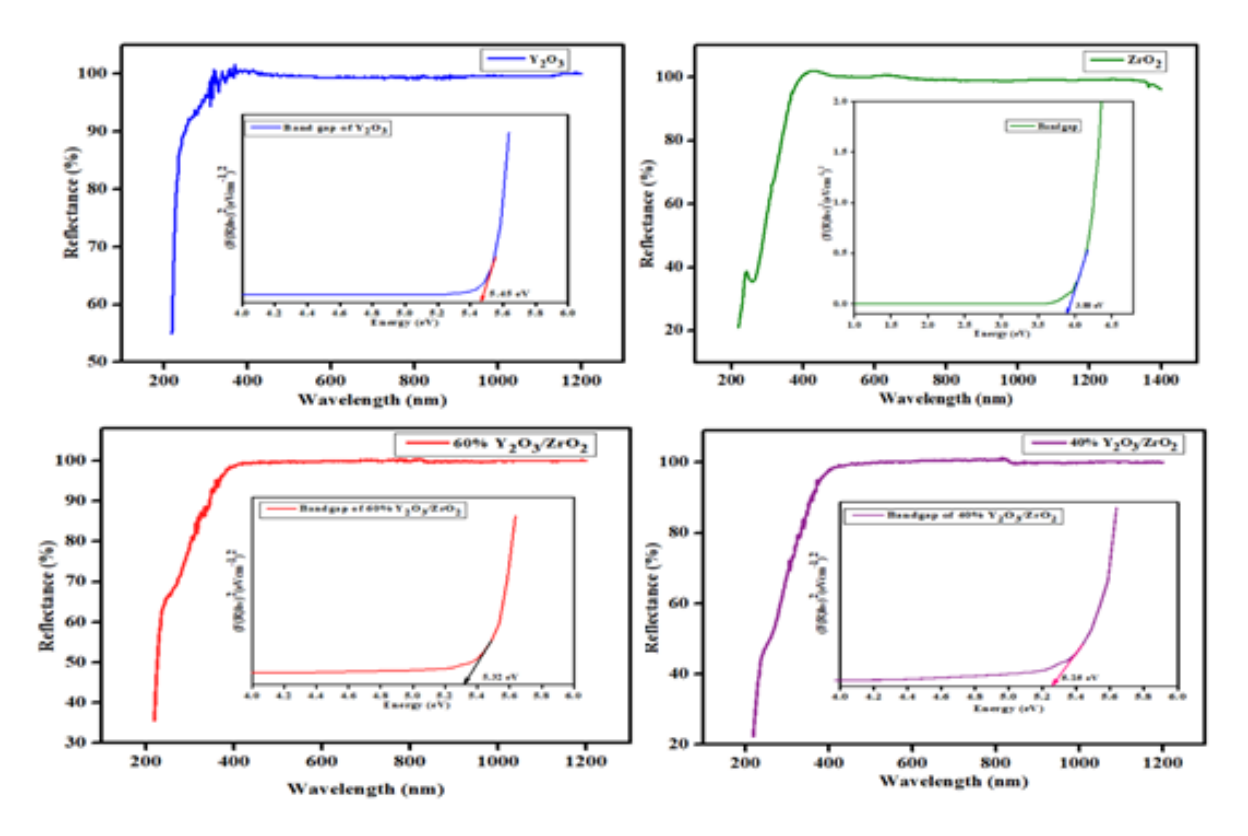


Figure 2. UV-Vis. spectrum of Pure Y₂O₃, 40% Y₂O₃/ZrO₂, 60% Y₂O₃/ZrO₂, Pure ZrO₂

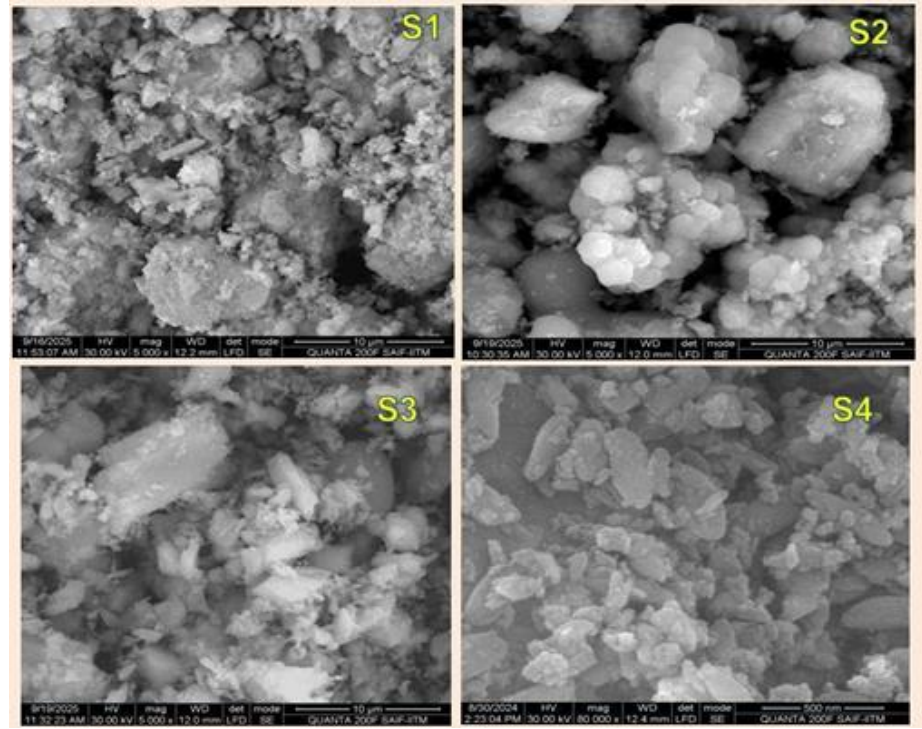


Figure 4. SEM images of Pure Y₂O₃ (S1), 40% Y₂O₃/ZrO₂ (S2), 60% Y₂O₃/ZrO₂ (S3), and pure ZrO₂ (S4).

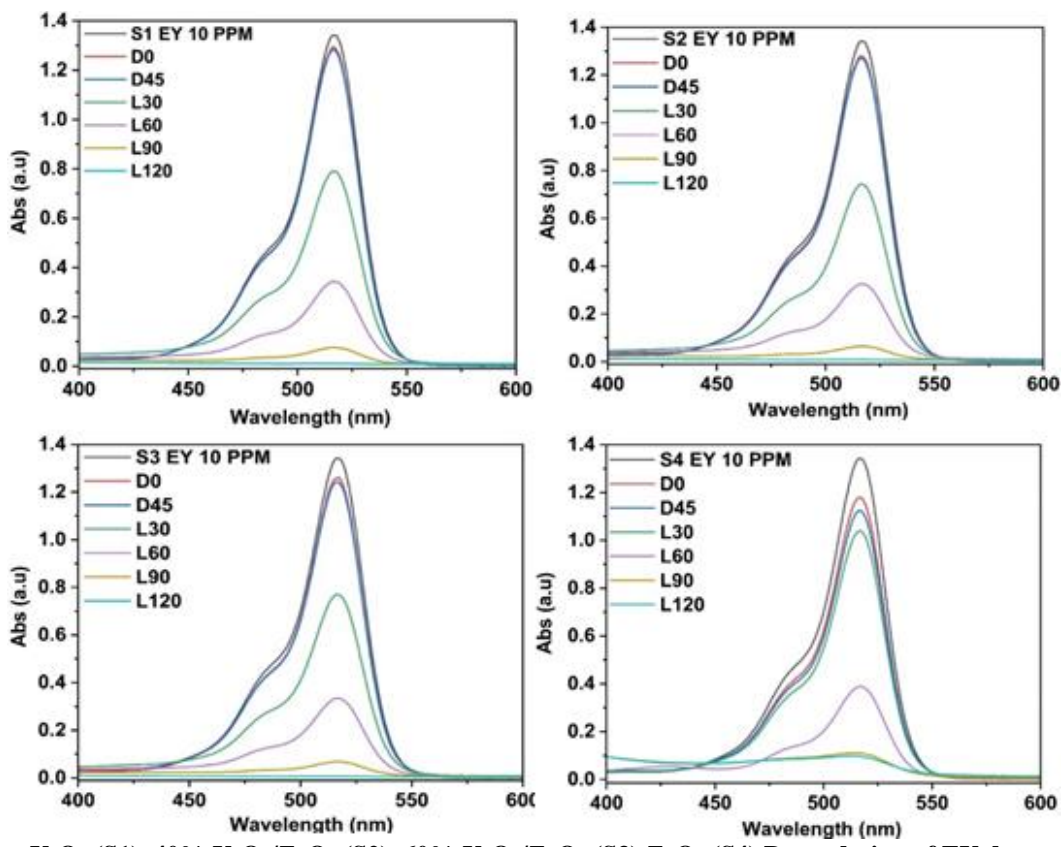


Figure 5. Pure Y₂O₃ (S1), 40% Y₂O₃/ZrO₂ (S2), 60% Y₂O₃/ZrO₂ (S3),ZrO₂ (S4) Degradation of EY dye at under visible light which shows degradation efficiency under concentration of 50mg.

4. Conclusion

In this work, pure zirconium oxide (ZrO_2) and yttrium oxide Y_2O_3 - ZrO_2 nanocomposite were successfully synthesized and comprehensively characterized to evaluate their structural, optical, photocatalytic, and antimicrobial properties. XRD analysis confirmed the crystalline nature of

the materials, revealing that Y_2O_3 -ZrO $_2$ induced a partial phase transformation and slightly reduced the average crystallite size. These structural modifications are beneficial for increasing surface area and improving the density of active sites for photocatalytic reactions. UV–Vis DRS studies showed that Y_2O_3 -ZrO $_2$ composite caused a red-shift in the absorption

edge, resulting in a slight bandgap narrowing. This bandgap reduction enhanced light harvesting in the near-UV region, enabling more efficient generation of photoinduced charge carriers. FTIR analyses provided further evidence of successful formation of composite by confirming the presence of Y–O and Zr-O vibrations, oxygen vacancies, and increased surface hydroxyl groups. These surface modifications play a crucial role in trapping charge carriers, reducing recombination, and facilitating the formation of reactive oxygen species (ROS).

Photocatalytic degradation experiments demonstrated that Y₂O₃-ZrO₂ composite exhibited superior photocatalytic performance for eosin yellow dye, as evidenced by higher degradation efficiency and faster reaction kinetics for model organic pollutants. The enhanced activity was attributed to improved light absorption, oxygen vacancy-mediated charge separation, and increased surface hydroxylation that favors •OH radical generation. The proposed photocatalytic mechanism highlighted the synergistic role of Y3+ and Zr4+ ions stabilizing the high-temperature phases, introducing defect states, and prolonging electron-hole lifetimes, resulting in more efficient ROS production. Overall, the combined structural, optical, photocatalytic, and antibacterial results confirm that Y₂O₃-ZrO₂ composite significantly improves the multifunctional performance than pure. The enhanced photocatalytic make $Y_2O_3-ZrO_2$ nanocomposites promising candidates for applications in wastewater treatment, environmental remediation, self-cleaning coatings, and biomedical surfaces requiring simultaneous contaminant degradation and microbial control.

References

- 1. Vassilenko, E.; Watkins, M.; Chastain, S.; Mertens, J.; Posacka, A.M.; Patankar, S.; Ross, P.S. Domestic laundry and microfiber pollution: Exploring fiber shedding from consumer apparel textiles. PLoS ONE 2021, 16, e0250346.
- 2.Roscam, A.M. Plastic Soup: An Atlas of Ocean Pollution; Island Press: Washington, DC, USA; Covelo, CA, USA; London, OH, USA, 2019; ISBN 10: 1642830089.
- 3. Waring, R.H.; Harrisa, R.M.; Mitchell, S.C. Plastic contamination of the food chain: A threat to human health? Maturitas 2018, 115, 64–68.
- 4.Black, O.; Smith, S.C.; Roper, C. Advances and limitations in the determination and assessment of gunshot residue in the environment. Ecotoxicol. Environ. Saf. 2021, 208, 111689.
- 5.Hassaan, M.A.; Nemr, A.E. Pesticides pollution: Classifications, human health impact, extraction and treatment techniques. Egypt. J. Aquat. Res. 2020, 46, 207–220.
- 6.Hansen, É.; Monteiro de Aquim, P.; Hansen, A.W.; Cardoso, J.K.; Ziulkoski, A.L.; Gutterres, M. Impact of post-tanning chemicals on the pollution load of tannery wastewater. J. Environ. Manag. 2020, 269, 110787.
- 7. Vasseghian, Y.; Khataee, A.; Dragoi, E.-N.; Moradi, M.; Nabavifard, S.; Conti, G.O.; Khaneghah, A.M. Pollutants degradation and power generation by photocatalytic fuel cells: A comprehensive review. Arab. J. Chem. 2020, 13, 8458–8480.
- 8.Eom, S.-Y.; Choi, J.; Bae, S.; Lim, J.-A.; Kim, G.-B.; Yu, S.-D.; Kim, Y.; Lim, H.-S.; Son, B.-S.; Paek, D.; et al. Health effects of environmental pollution in population living near

- industrial complex areas in Korea. Environ. Health Toxicol. 2018, 33, e2018004.
- 9.Gupta, A.K. Thermal Destruction of Solid Wastes. ASME J. Energy Resour. Technol. 1996, 118, 187–192.
- 10.Tornevi, A.; Bergstedt, O.; Forsberg, B. Precipitation Effects on Microbial Pollution in a River: Lag Structures and Seasonal EffectModification. PLoS ONE 2014, 9, e98546.
- 11.Dharupaneedi, S.P.; Nataraj, S.K.; Nadagouda, M.; Reddy, K.R.; Shukla, S.S.; Aminabhavi, T.M. Membrane-based separation ofpotential emerging pollutants. Sep. Purif. Technol. 2019, 210, 850–866.
- 12.Hussain, C.M.; Paulraj, M.S.; Nuzhat, S. Chapter 2 Source reduction, waste minimization, and cleaner technologies. In SourceReduction and Waste Minimization; Elsevier: Amsterdam, The Netherlands, 2022; pp. 23–59. ISBN 9780128243206.
- 13.Usharani, B.; Murugadoss, G.; Rajesh Kumar, M.; GousePeera, S.; Manivannan, V. Reduced Graphene Oxide–Metal Oxide Nanocomposites (ZrO₂ and Y₂O₃): Fabrication and Characterization for the Photocatalytic Degradation of Picric Acid. *Catalysts* 2022, *12*, 1249.
- 14.Ju, Meng and Pan, Lu and Zhang, Chuanzhao and Jin, Yuanyuan and Zhong, Mingmin and Li, Song and Li, Shichang and Yang, Tie and Wang, Xiaotian, The geometrical structure and electronic properties of trivalent Ho3+ doped Y2O3 crystals: a first-principles study, RSC Adv., (2020), volume 10, pages 28674-28679,
- 15. Moosavi, S.; Lai, C.W.; Gan, S.; Zamiri, G.; Pivehzhani, O.A.; Johan, M.R. Application of Efficient Magnetic Particles and ActivatedCarbon for Dye Removal fromWastewater. ACS Omega 2020, 5, 20684–20697.
- 16.Majid, Z.; Razak, A.A.; Noori, W.A.H. Modification of Zeolite by Magnetic Nanoparticles for Organic Dye Removal. Arab. J. Sci.Eng. 2019, 44, 5457–5474.
- 17. Watwe, V.S.; Kulkarni, S.D.; Kulkarni, P.S. Cr (VI)-Mediated Homogeneous Fenton Oxidation for Decolorization of Methylene Blue Dye: Sludge Free and Pertinent to a Wide pH Range. ACS Omega 2021, 6, 27288–27296.
- 18.Sarkar, S.; Ponce, N.T.; Banerjee, A.; Bandopadhyay, R.; Rajendran, S.; Lichtfouse, E. Green polymeric nanomaterials for the photocatalytic degradation of dyes: A review. Environ. Chem. Lett. 2020, 18, 1569–1580.
- 19. Casimiro, F.M.; Costa, C.A.E.; Botelho, C.M.; Barreiro, M.F.; Rodrigue, A.E. Kinetics of Oxidative Degradation of Lignin-BasedPhenolic Compounds in Batch Reactor. Ind. Eng. Chem. Res. 2019, 58, 16442–16449.
- 20.Polisetti, S.; Deshpande, P.A.; Madras, G. Photocatalytic Activity of Combustion Synthesized ZrO_2 and ZrO_2 – TiO_2 Mixed Oxides.Ind. Eng. Chem. Res. 2011, 50, 12915–12924. 21.Basahel, S.N.; Ali, T.T.; Mokhtar, M.; Narasimharao, K. Influence of crystal structure of nanosized ZrO_2 on photocatalytic degradation of methyl orange. Nanoscale Res. 2015, 10, 73.